*Supporting Information for:*

# Mechanism of a Class C Radical SAM Thiazole Methyl Transferase

Zhengan Zhang,[1,2] Nilkamal Mahanta,[1,3] Graham A. Hudson,[1] Douglas A. Mitchell[1,3]*

and Wilfred A. van der Donk[1-3]*

[1] Department of Chemistry, University of Illinois at Urbana-Champaign, Urbana, Illinois 61801, USA. [2] Howard Hughes Medical Institute, University of Illinois at Urbana-Champaign, Urbana, Illinois 61801, [3] Institute for Genomic Biology, University of Illinois at Urbana-Champaign, 1206 West Gregory Drive, Urbana, IL, 61801, USA.

* Corresponding authors:
Wilfred A. van der Donk (vddonk@illinois.edu), phone: 1-217-244-5360, fax: 1-217-244-8533
Douglas A. Mitchell (douglasm@illinois.edu), phone: 1-217-333-1345, fax: 1-217-333-0508

## Table of Contents:

## Supporting Figures

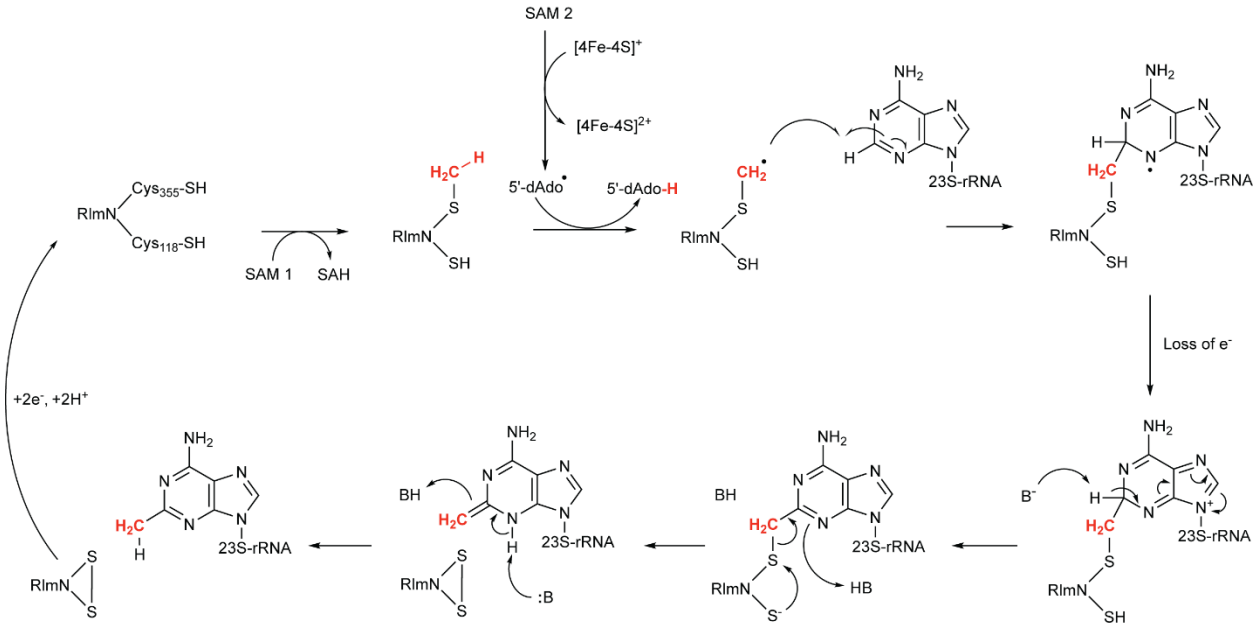


**Figure S1. Mechanism of class A rSAM MT RlmN.**[1] RlmN methylates an adenine in 23S-tRNA by first methylating a Cys in the enzyme, and then using 5'-dA• derived from a second SAM to abstract a hydrogen atom from the methylated Cys. The resulting radical is added to the adenine, and oxidized to a cation. Deprotonation generates a neutral intermediate that is resolved by disulfide bond formation. Since RlmN does not formally transfer a methyl group, but rather a methylene group, class A rSAM MTs could be referred to as methylases.

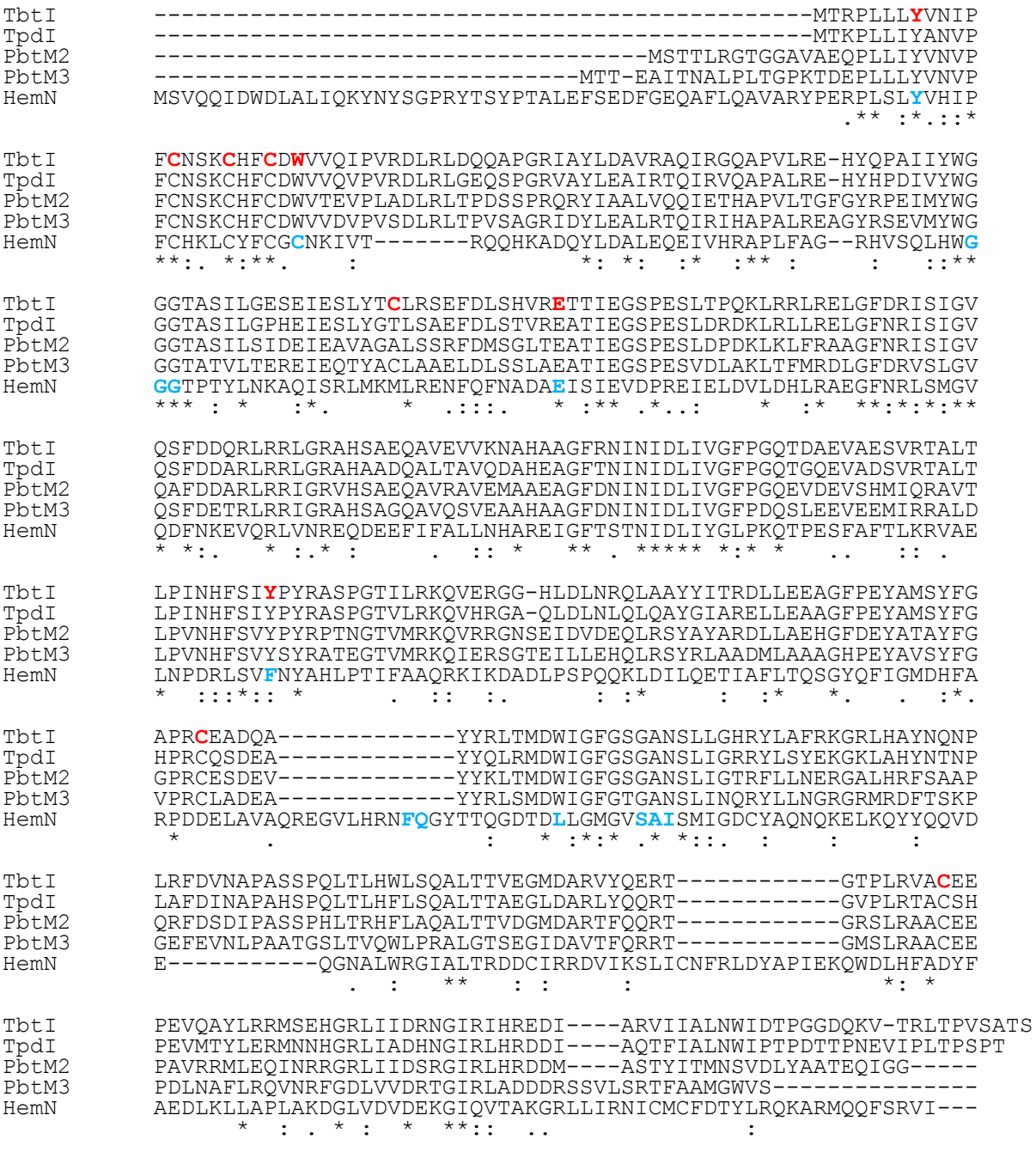


**Figure S2. Sequence alignment of select class C rSAM MTs.** Proteins shown include TbtI from the hypothetical thiomuracin producer *Thermobispora bispora* (WP_013130805.1), TpdI from known thiomuracin producer *Nonomuraea* sp. Bp3714-39 (ACS83777.1), PbtM2/M3 from GE2270A producer *Nonomuraea* sp. WU8817 (AGY49586.1/AGY49595.1), and HemN from *Escherichia coli* (WP_001502804.1). Cys residues involved in [4Fe-4S] cluster formation are highlighted yellow. TbtI residues chosen for Ala substitution are shown in red. HemN residues within 5 Å of SAM2 are shown in blue.

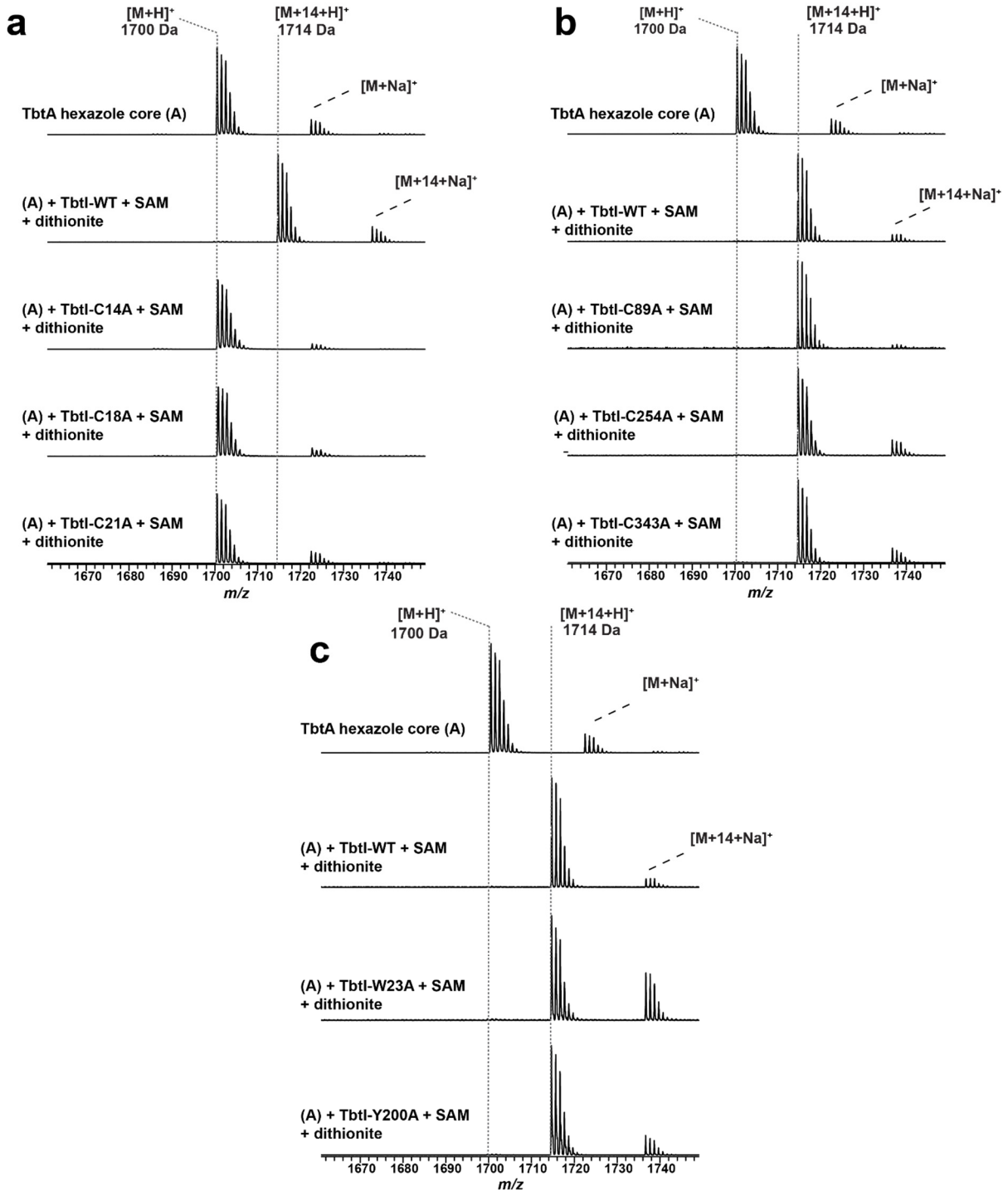


**Figure S3. MALDI-TOF MS analysis of the products generated by TbtI variants. (a)** Spectra of TbtA hexazole treated with wild type (wt) TbtI or TbtI variants in which the Cys residues expected to be involved in binding to the [4Fe-4S] cluster were substituted with Ala. **(b)** Spectra of TbtA hexazole treated with wt TbtI or TbtI variants in which the remaining Cys residues were substituted with Ala. **(c**) Spectra of TbtA hexazole treated with wt TbtI or variants in which conserved Tyr/Trp residues were individually substituted with Ala without loss of activity. Very similar results were obtained for the Cys variants when DTT was removed from the assays.

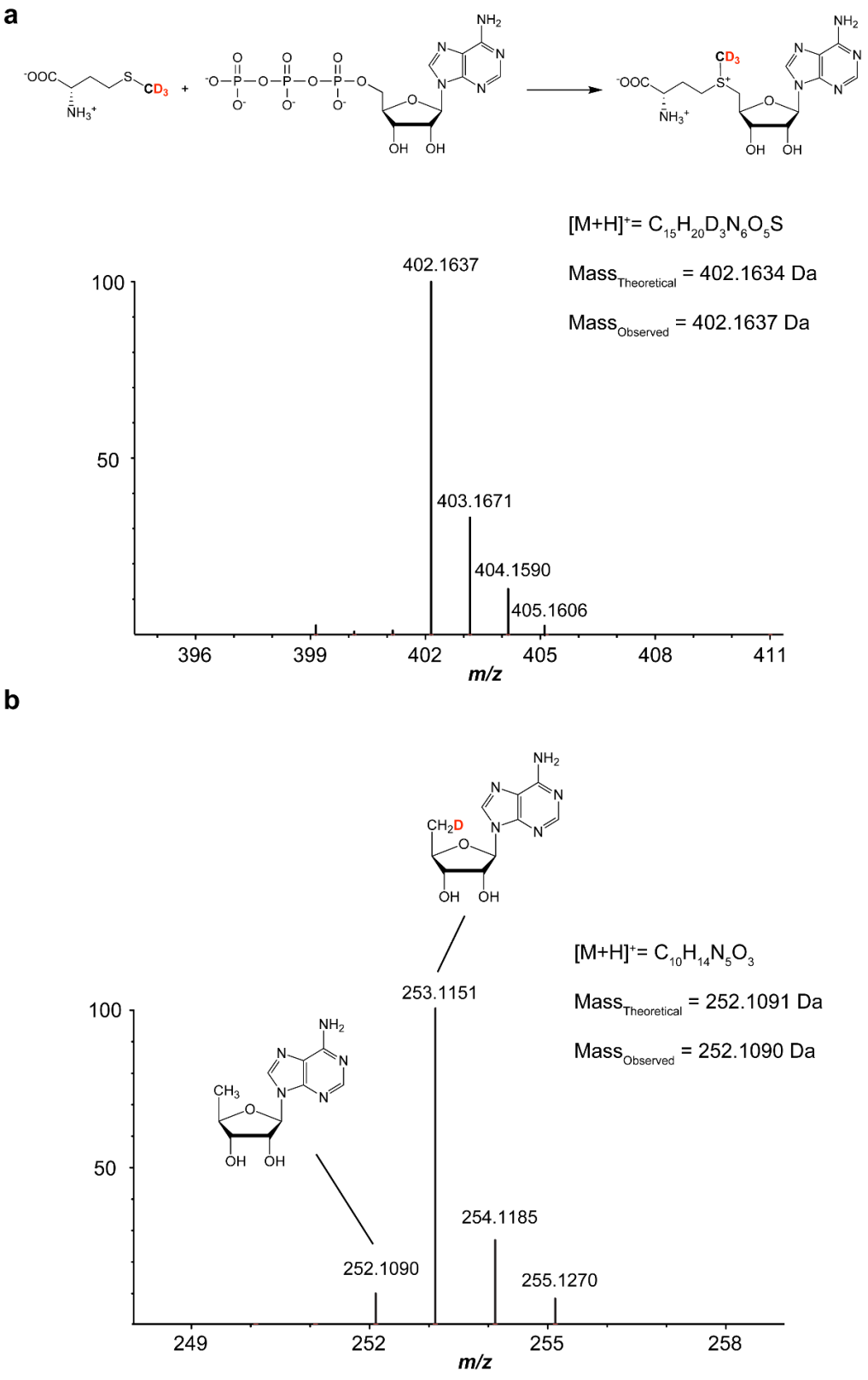


**Figure S4. (a)** ESI-MS of the $CD_3$-SAM starting material. Error, 0.7 ppm. **(b)** ESI-MS analysis of 5'-dA produced during the methylation of TbtA by TbtI in the presence of $CD_3$-SAM. Error, 0.4 ppm. The deuterium content of $CD_3$-SAM was calculated as follows: (Peak intensity$_{m/z = 402}$)/ [(Peak intensity$_{m/z = 402}$) + (Peak intensity$_{m/z = 399}$)+ (Peak intensity$_{m/z = 400}$)+ (Peak intensity$_{m/z = 401}$)].

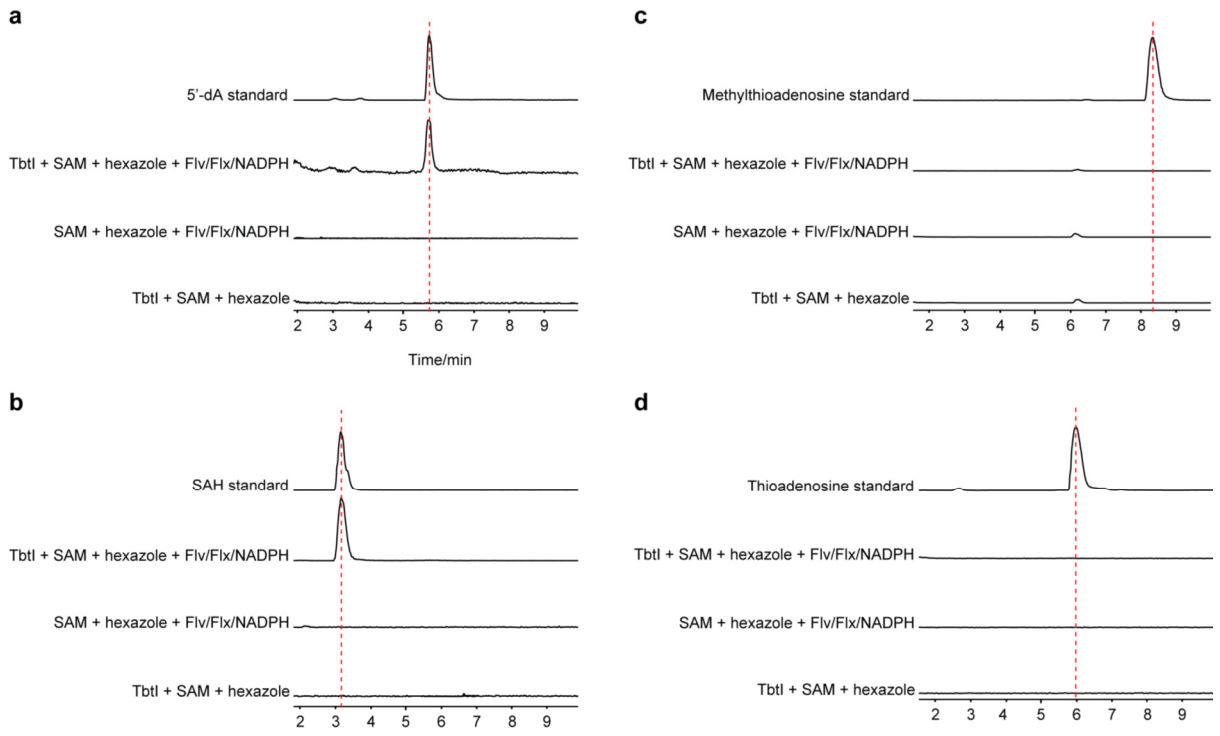


**Figure S5. Products of the TbtI reaction. (a-b)** Extracted ion chromatograms to analyze production of 5'-dA and SAH showed their generation was dependent on the presence of both TbtI and the reducing system. **(c-d)** Extracted ion chromatograms to analyze potential production of methylthioadenosine and thioadenosine did not show the presence of these products under the reaction conditions.

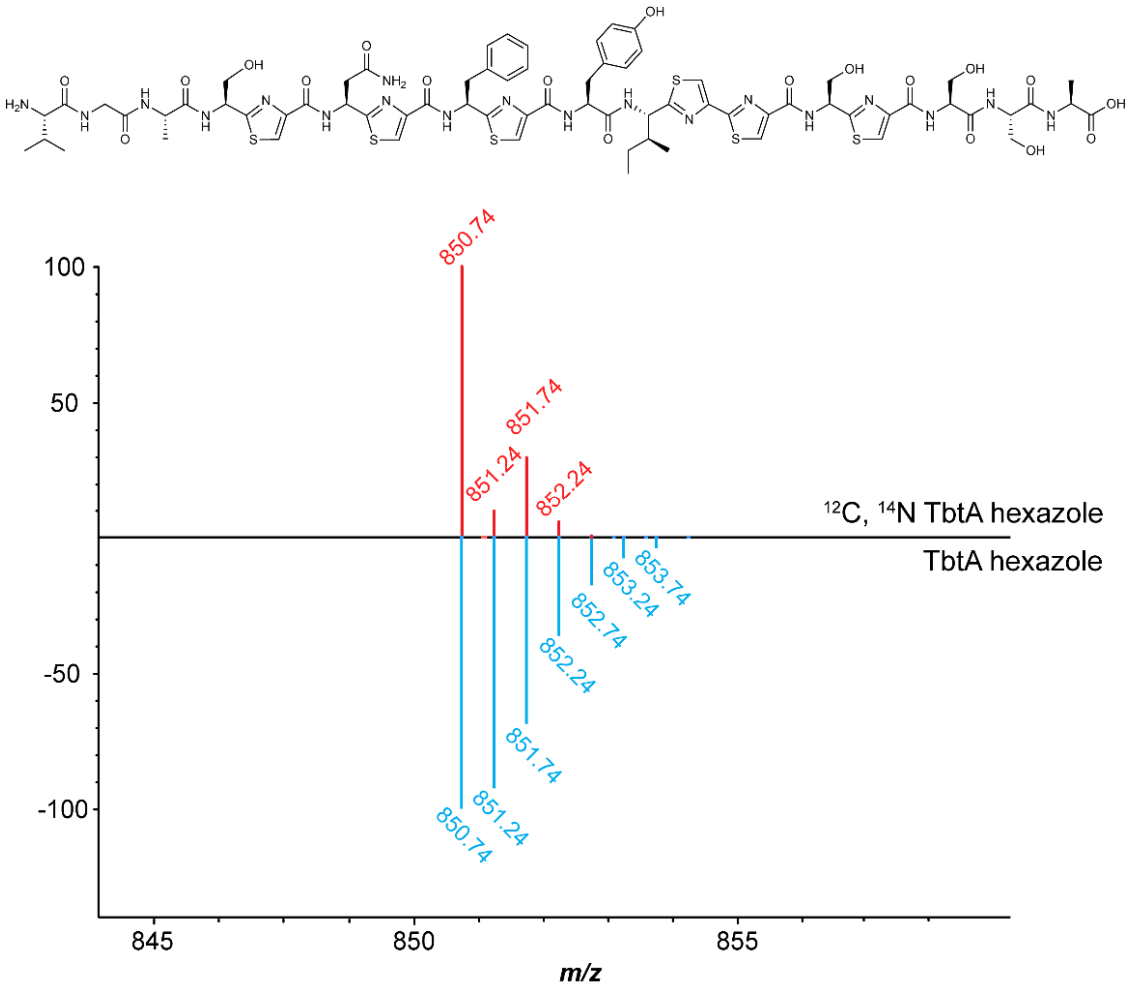


**Figure S6.** ESI-MS analysis of the doubly charged ($^{13}C$, $^{15}N$)-depleted TbtA hexazole **1** (top, red) and natural abundance TbtA hexazole (bottom, blue). See Table S2 for calculated and observed masses.

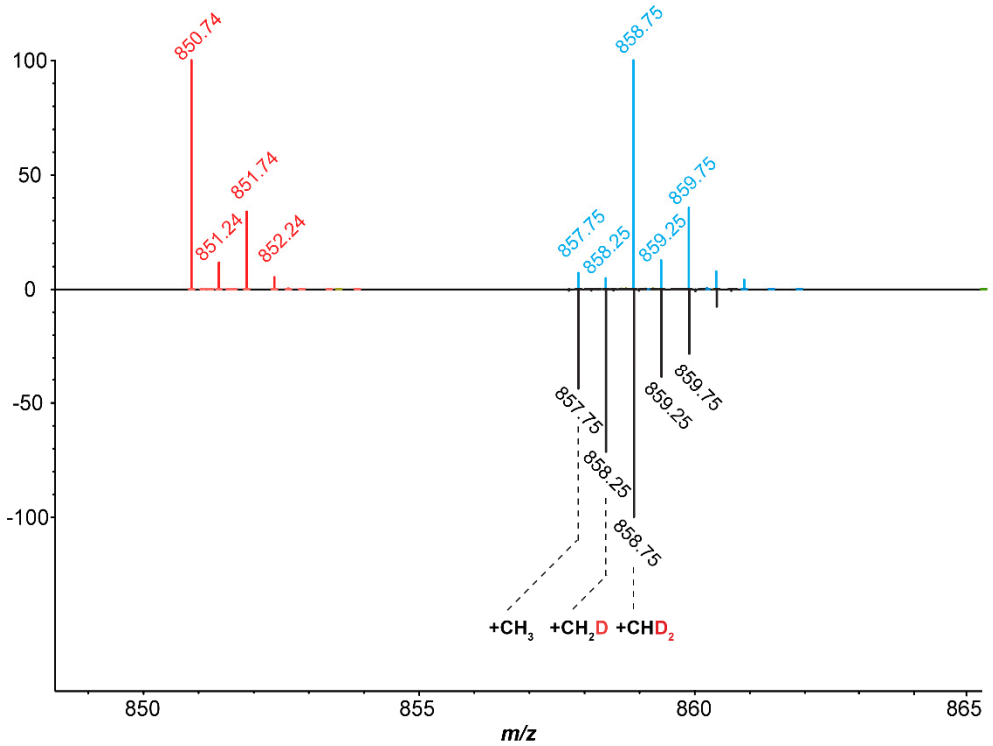


**Figure S7. ESI-MS spectra to investigate methyl group solvent exchange**. Spectra showing the doubly charged core peptide of the TbtA hexazole substrate (red) and product obtained with $CD_3$-SAM in $H_2O$ after a 1 h reaction (blue) or the product from this reaction re-exposed to the same reaction for 16 h (black). See Table S2 for calculated and observed masses.

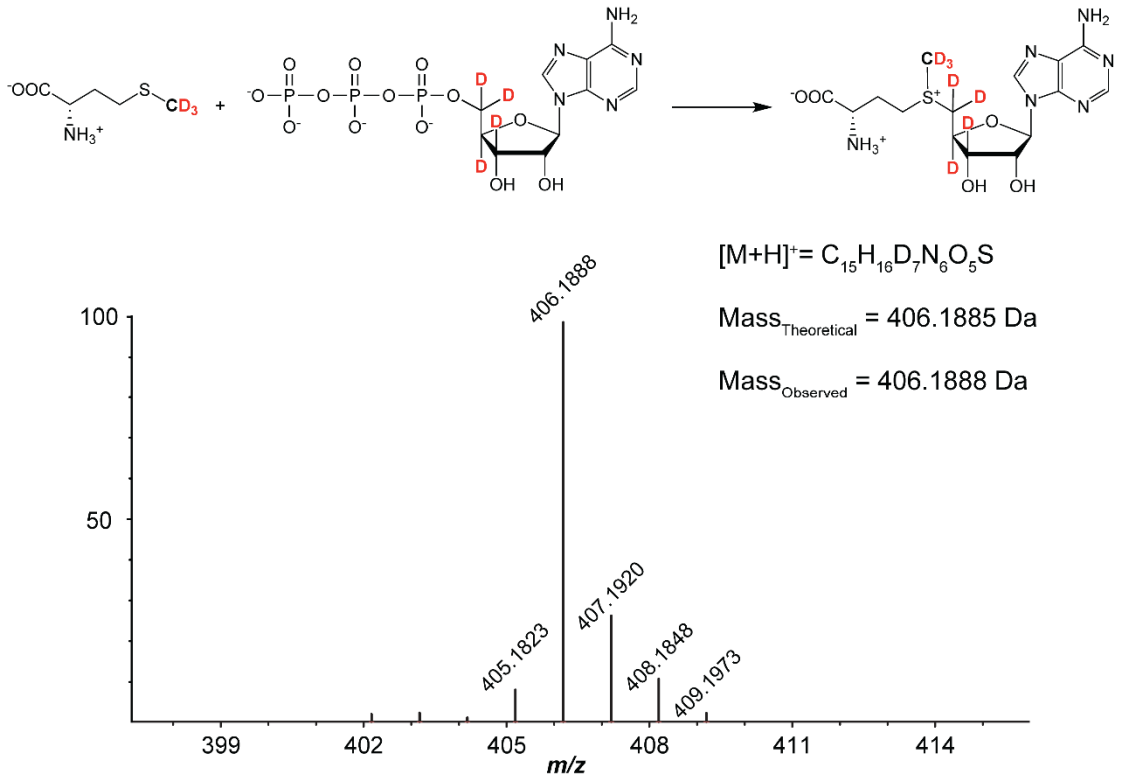


**Figure S8. Synthesis and ESI-MS analysis of $CD_3$-5',5',4',3'-$D_4$-SAM.** Error, 0.7 ppm. The deuterium content of $CD_3$-5',5',4',3'-$D_4$-SAM was calculated as follows taking into account that some of the ion at 406 might arise from a $^{13}$C-contaning isotopologue of the ion at m/z 405: [(Peak intensity$_{m/z = 406}$) − (0.3 × Peak intensity$_{m/z = 405}$)/ [(Peak intensity$_{m/z = 406}$) + (Peak intensity$_{m/z = 405}$) + (Peak intensity$_{m/z = 404}$) + (Peak intensity$_{m/z = 403}$) + (Peak intensity$_{m/z = 402}$)].

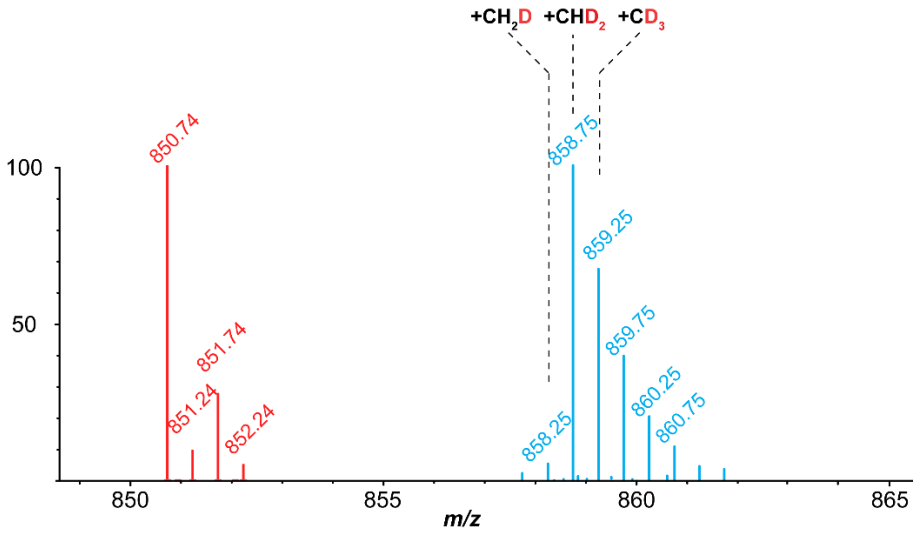


**Figure S9. ESI-MS spectra ruling out transfer of a non-exchangeable hydrogen derived from the protein.** Spectra showing the doubly charged core peptide of the TbtA hexazole substrate **1** (red) and product obtained with a 20-fold excess of substrate and $CD_3$-SAM with TbtI in buffered $D_2O$.

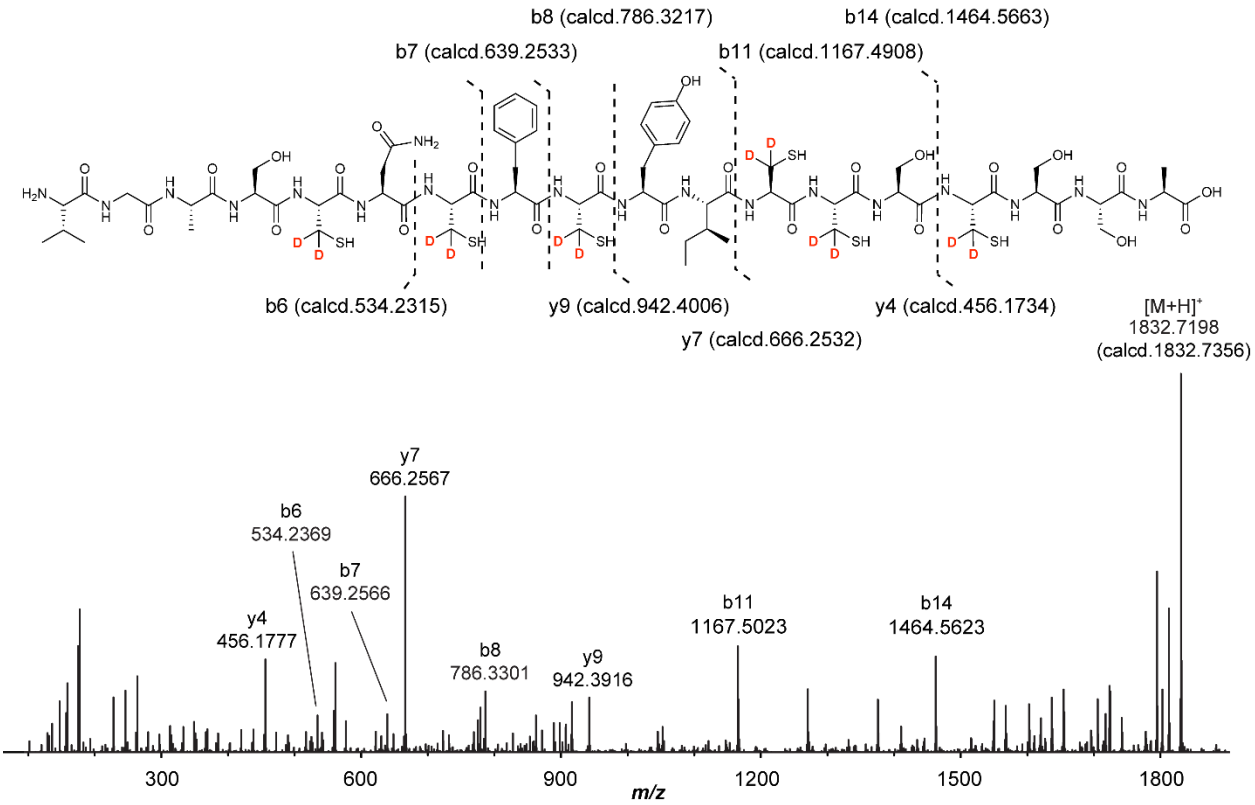


| Species | Predicted mass | Observed mass | Error (ppm) |
|---|---|---|---|
| $[M+H]^+$ | 1832.7356 | 1832.7198 | 8.6 |
| b6 | 534.2315 | 534.2369 | 10.1 |
| b7 | 639.2533 | 639.2566 | 5.2 |
| b8 | 786.3217 | 786.3301 | 10.7 |
| b11 | 1167.4908 | 1167.5023 | 9.9 |
| b14 | 1464.5663 | 1464.5623 | 2.7 |
| y4 | 456.1734 | 456.1777 | 9.4 |
| y7 | 666.2532 | 666.2567 | 5.3 |
| y9 | 942.4006 | 942.3916 | 9.6 |

**Figure S10. Tandem ESI-MS on TbtA core peptide containing six $D_2$-Cys residues.** The tandem MS analysis was performed on the precursor peptide pre-treated with endoproteinase GluC to remove most of the leader peptide.[2] Analysis of the tandem MS data reveals that six $D_2$-Cys were incorporated into the peptide. The deuterium content at Cys4 was estimated by determining the deuterium content of the b7 ion in comparison to the deuterium content of the b6 ion: [peak intensity of the $b_7$ ion ($m/z$ = 639)/ (peak intensity of the $b_7$ ion ($m/z$ = 639) + the peak intensity of b7 − 1 ion ($m/z$ = 638))] – [peak intensity of the $b_6$ ion ($m/z$ = 534)/ (peak intensity of the $b_6$ ion ($m/z$ = 534) + the peak intensity of b6 − 1 ion ($m/z$ = 533))].

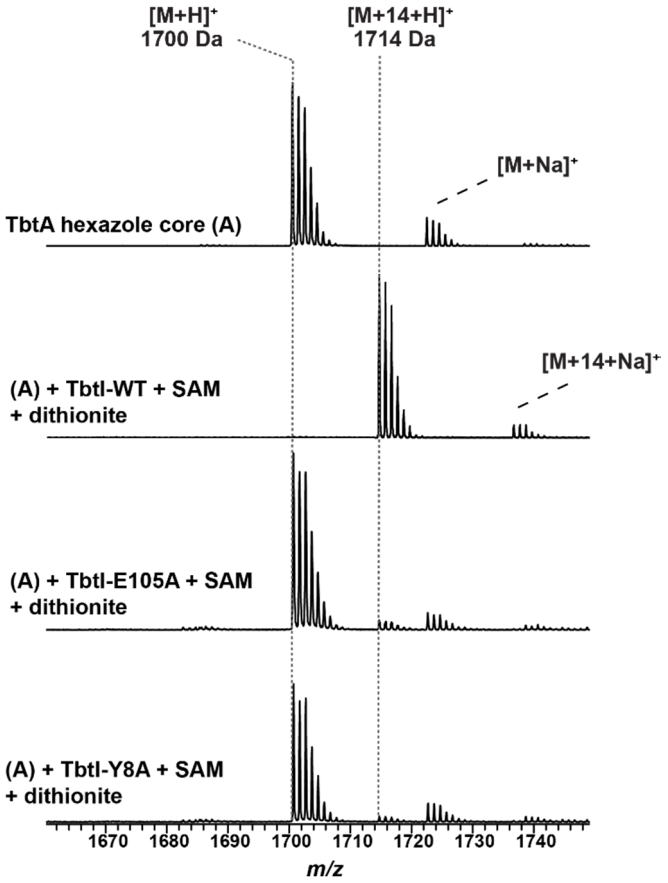


**Figure S11. MALDI-TOF MS analysis of the products generated by TbtI variants.** Spectra of TbtA treated with wt TbtI or TbtI variants in which the class C rSAM-conserved Glu and Tyr residues were substituted with Ala. According to the crystal structure of HemN, these residues are near the SAM-binding site.

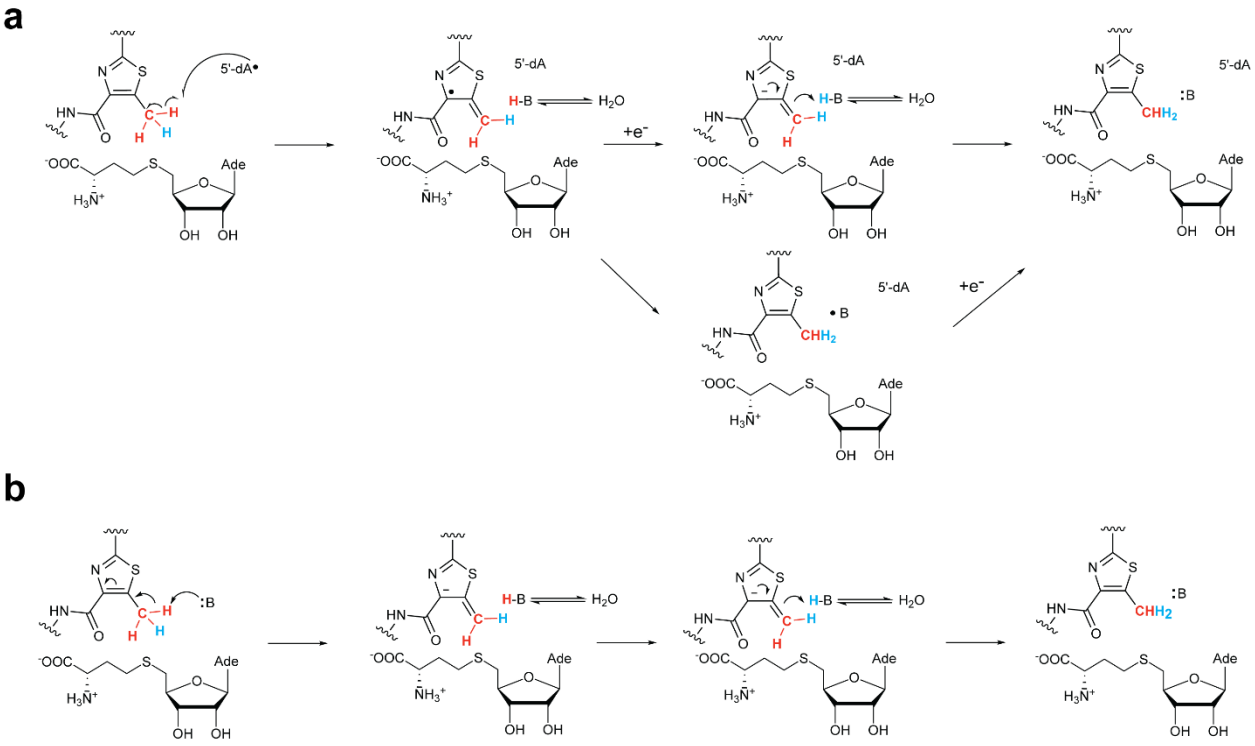


**Figure S12. Proposed mechanisms for exchange of the methyl protons of the product peptide. (a)** The methylated product and SAH can bind to the enzyme, SAM1 can be cleaved to initiate the hydrogen atom abstraction from the methylated peptide. Its methyl group would be expected to occupy a very similar position as the methyl group of SAM2 during normal turnover. Reduction of the resulting radical to the anion and protonation results in exchange (analogous to pathway *a* in Figure 2), or hydrogen atom abstraction from a redox active residue in the active site (analogous to pathway *b*, Figure 2) would result in exchange. **(b)** An alternative mechanism involves deprotonation of the methyl group, the reverse of the protonation step that provides the product in pathway *a*. The mechanism in panel **(a)** requires SAM cleavage whereas the mechanism in **(b)** does not. Unfortunately, we were not able to determine whether a hydrogen is transferred from the methyl group to 5'-dA during prolonged reactions because of extensive abortive SAM cleavage. Ade = adenine.

**Table S1. Oligonucleotide primers used in this study**. All sequences are provided 5′ to 3′. F indicates a forward primer while R indicates the reverse primer.

| Primer Name | Oligonucleotide Sequence |
|---|---|
| *tbtI* C14A F | ATATCCCGTTCGCTAACTCTAAATGCCACTTCTGCGACTGG |
| *tbtI* C14A R | CATTTAGAGTTAGCGAACGGGATATTCACATACAGCAGCAG |
| *tbtI* C18A F | GTAACTCTAAAGCCCACTTCTGCGACTGGGTTGTCCAAATC |
| *tbtI* C18A R | TCGCAGAAGTGGGCTTTAGAGTTACAGAACGGGATATTCAC |
| *tbtI* C21A F | AATGCCACTTCGCCGACTGGGTTGTCCAAATCCCGGTGCGT |
| *tbtI* C21A R | ACAACCCAGTCGGCGAAGTGGCATTTAGAGTTACAGAACGG |
| *tbtI* C89A F | CTCTGTATACGGCCCTGCGTTCAGAATTCGATCTGTCGCAC |
| *tbtI* C89A R | TCTGAACGCAGGGCCGTATACAGAGATTCGATTTCGCTTTC |
| *tbtI* C254A F | GTGCACCGCGTGCCGAAGCAGATCAGGCATATTACCGCCTG |
| *tbtI* C254A R | TGATCTGCTTCGGCACGCGGTGCACCGAAGTAGCTCATCGC |
| *tbtI* C343A F | TGCGTGTCGCAGCTGAAGAACCGGAAGTGCAAGCCTACCTG |
| *tbtI* C343A R | TCCGGTTCTTCAGCTGCGACACGCAGCGGCGTACCGGTACGT |
| *tbtI* W23A F | ACTTCTGCGACGCGGTTGTCCAAATCCCGGTGCGTGATCTG |
| *tbtI* W23A R | ATTTGGACAACCGCGTCGCAGAAGTGGCATTTAGAGTTACA |
| *tbtI* Y200A F | ATTTTAGTATCGCTCCGTACCGTGCATCCCCGGGTACCATT |
| *tbtI* Y200A R | GCACGGTACGGAGCGATACTAAAATGGTTAATCGGCAGCGT |
| *tbtI* E105A F | AAACCACGATTGCAGGTAGTCCGGAATCCCTGACCCCGCAG |
| *tbtI* E105A R | TCCGGACTACCTGCAATCGTGGTTTCGCGGACGTGCGACAG |
| *tbtI* Y8A F | CGCTGCTGCTGGCTGTGAATATCCCGTTCTGTAACTCTAAA |
| *tbtI* Y8A R | GGGATATTCACAGCCAGCAGCAGCGGGCGCGTCAT |

**Table S2: Expected and observed masses in Figures 3, 4, S5, and S6.** Each species listed below is doubly charged.

| Species | Calculated mass (Da) | Observed mass (Da) | Error (ppm) |
|---|---|---|---|
| Hexazole | 850.7369 | 850.7380 | 1.3 |
| Hexazole + $CH_3$ | 857.7448 | 857.7416 | 3.7 |
| Hexazole + $CH_2D$ | 858.2479 | 858.2437 | 4.9 |
| Hexazole + $CHD_2$ | 858.7510 | 858.7507 | 0.3 |
| Hexazole + $CD_3$ | 859.2542 | 859.2537 | 0.6 |
| $D_6$-Hexazole | 853.7558 | 853.7578 | 2.4 |
| $D_6$-Hexazole + $CH_3$ - D | 860.2605 | 860.2607 | 0.3 |
| $D_6$-Hexazole + $CH_2D$ - D | 860.7636 | 860.7611 | 2.9 |
| $D_6$-Hexazole + $CHD_2$ - D | 861.2667 | 861.2658 | 1.1 |
| $D_6$-Hexazole + $CD_3$ - D | 861.7699 | 861.7624 | 8.7 |

**Supporting References**

(1) Grove, T. L.; Livada, J.; Schwalm, E. L.; Green, M. T.; Booker, S. J.; Silakov, A. *Nat. Chem. Biol.* **2013**, *9*, 422.
(2) Hudson, G. A.; Zhang, Z.; Tietz, J. I.; Mitchell, D. A.; van der Donk, W. A. *J. Am. Chem. Soc.* **2015**, *137*, 16012.